Journal of Materials Chemistry C

Strong electron-phonon coupling driven charge density wave states in stoichiometric 1T-VS_2 crystals

Journal:	*Journal of Materials Chemistry C*
Manuscript ID	TC-COM-10-2022-004186.R1
Article Type:	Communication
Date Submitted by the Author:	25-Oct-2022
Complete List of Authors:	Lee, Si-Hong; DGIST Park, Yun Chang; National Nanofab Center, Chae, Jinwoong; Sejong University, Department of Physics and Astronomy Kim, Gunn; Sejong University, Physics Kim, Hyuk Jin; University of Seoul Choi, Byoung Ki; University of Seoul, Department of Physics Lee, In Hak; Korea Institute of Science and Technology Chang, Young Jun; University of Seoul, Department of Physics Chun, Seung-Hyun; Sejong University, Department of Physics Jung, Minkyung; DGIST, Research Institute Seo, Jungpil; Daegu Gyeongbuk Institute of Science & Technology, Department of Emerging Materials Science Lee, Sunghun; Sejong University, Department of Physics and Astronomy

Strong electron-phonon coupling driven charge density wave states in stoichiometric 1T-VS_2 crystals

*Si-Hong Lee,[a] Yun Chang Park,[b] Jinwoong Chae,[c,d] Gunn Kim,[c,d] Hyuk Jin Kim,[e] Byoung Ki Choi,[e,f] In Hak Lee,[e,g] Young Jun Chang,[e,h] Seung-Hyun Chun,[c] Minkyung Jung,[i] Jungpil Seo,[*a] Sunghun Lee[*c]*

[a]Department of Physics and Chemistry, DGIST, Daegu 42988, Korea.

[b]Department of Measurement and Analysis, National Nanofab Center, Daejeon 34141, Korea.

[c]Department of Physics and Astronomy, Sejong University, Seoul 05006, Korea.

[d]Hybrid Materials Research Center, Sejong University, Seoul 05006, Korea.

[e]Department of Physics, University of Seoul, Seoul 02504, Korea.

[f]Advanced Light Source (ALS), E. O. Lawrence Berkeley National Laboratory, Berkeley, CA, United States.

[g]Center for Spintronics, Korea Institute of Science and Technology, Seoul 02792, Korea.

[h]Department of Smart Cities, University of Seoul, Seoul 02504, Korea.

[i]DGIST Research Institute, DGIST, Daegu 42988, Korea.

*Corresponding authors email; jseo@dgist.ac.kr (J.S). kshlee@sejong.ac.kr (S.L.)

KEYWORDS: Vanadium disulfide, 1T phase, Vacuum annealing treatment, Charge density wave transition, Electron-phonon coupling

ABSTRACT

A charge density wave (CDW) transition is one of the fundamental quantum phenomena used to unveil the interactions between electrons and phonons that are coexisting or competing with other intriguing quantum phases, such as superconducting and ferromagnetic phases. Layered van der Waals materials, especially the family of vanadium dichalcogenides (VS_2, VSe_2, and VTe_2), have previously demonstrated CDW transition and ferromagnetic ordering, although these demonstrations lacked critical evidence. Among them, VS_2 single crystals in bulk form are challenging materials due to their thermodynamical instability; thus, experiments involving these materials have been rare. Herein, we report the multiple CDW states of a perfect 1T-phase VS_2 single crystal fabricated by chemical vapor transport and annealing treatment. The metastable phase comprising VS_2 and V_5S_8 turned into a stoichiometric 1T-phase VS_2 single crystal, confirmed by high-resolution microscopy. The fine structure formed at low temperature exhibits two clear CDW orders with the absence of nesting vectors on the Fermi surface, confirmed by scanning tunneling microscopy and density functional theory calculations. Our findings provide insight into obtaining a stable crystallographic phase of VS_2, stimulating further research into its compelling physical properties.

Introduction

Two-dimensional (2D) materials, including transition metal dichalcogenides (TMDCs), have provided novel opportunities to explore and manipulate their electronic states.[1-4] The unique properties of the quasi-2D electronic states of TMDCs can produce diverse physical phenomena, such as charge density waves (CDWs), superconductivity, ferromagnetism, topological Dirac states, and Mott-insulator transitions, in various polymorphic phases.[5-10] In particular, the CDW, a type of coupled electronic-lattice instability, permeates the condensed matter physics and chemistry due to broken symmetry states, where the atomic lattice and charge densities are spatially redistributed in a periodic structural order.[11,12] While the CDW transition is conventionally believed to arise from electronic instability driven by Fermi surface nesting,[13,14] electron-electron or electron-phonon interactions are dominant mechanisms in some 2D TMDC materials.[15,16] Recent studies suggest that the dimensionality and polymorphic phases of TMDC materials affect the formation of CDW.[14,17-19] However, the primary origin of the CDW transition is still under debate.

Vanadium (V)-based dichalcogenides (VS_2, VSe_2, and VTe_2) have been mainly investigated in electrochemical studies.[20-22] Recently, their intriguing physical properties, such as ferromagnetism, non-trivial band topology, and CDW, were reported, demonstrating their correlated nature.[23-27] In the bulk VSe_2, the nesting vectors that joins the flat segments of Fermi surface are responsible for the CDW transition at ~110 K.[28-30] Bulk VTe_2 shows more complicated charge ordering states than VSe_2, and the transition mechanism is not settled. VTe_2 undergoes a structural transition from 1T phase to 1T″ phase at ~480 K,[24,31,32] whose CDW transition could be polymorphic and coupled to the spin degree of freedom.[26] Since the CDW transition is sensitively dependent on a periodic and consistent atomic order, a high-quality crystal is imperative for understanding the CDW transition in bulk form.[33] However, the

experimental CDW results of VS_2 were fewer and more limited than those of VSe_2 and VTe_2 until now, owing to unstable stoichiometric VS_2 in bulk.[34,35] Thermodynamically stable VS_2 in the bulk form usually suffers from S-deficiency with self-intercalated V atoms between S layers.[36,37] Several studies have reported CDW transitions in VS_2 in several ways, but the observed transition temperatures (T_{CDW}) were different for this reason.[38-42] Thus, the synthesis of high-quality stoichiometric single crystals is imperative to understanding CDW formation in VS_2.

In this work, we report that a mixture of V_5S_8 and VS_2 bulk grown by the chemical vapor transport (CVT) method turned into stoichiometric VS_2 single crystals treated by low-temperature vacuum annealing. The as-fabricated VS_2 crystals were well-oriented along the *c*-axis and exhibited an apparent 1T trigonal structure, confirmed in both the top and side views of high-resolution electron microscopic images. We then investigated CDW formation based on these stoichiometric VS_2 single crystals using scanning tunneling microscopy (STM), exhibiting two distinct CDW orders. The nesting vectors in the two CDW states did not exist on the Fermi surface. To figure out the absence of nesting vectors, albeit clear CDW orders, we performed density functional theory (DFT) calculations and showed that the phonon modes around the two CDW vectors were significantly renormalized by electron-phonon coupling, inducing CDW instabilities.

Results and discussion

Since the stoichiometric phase of VS_2 sustains thermodynamic metastability,[36,43] in earlier studies, various methods, such as alkali-metal deintercalation and high-pressure synthesis, were performed to achieve stoichiometric VS_2.[44,45] In this work, 1T trigonal VS_2 was first grown by the CVT method, and then a low-temperature vacuum annealing treatment was

conducted, resulting in stoichiometric VS_2 bulk crystals. The detailed experimental process is described in the experimental method section. Fig. 1a depicts a schematic illustration of the VS_2 crystal growth process and the partial products (right photograph in Fig. 1a). Fig. 1b shows the XRD patterns of the as-grown VS_2 crystals before and after vacuum annealing treatment. The observed XRD spectrum before vacuum annealing treatment exhibited blended patterns of trigonal VS_2 (lattice parameters $a = b = 3.23$ Å and $c = 5.71$ Å, space group P-3m1, JCPDS card no. 04-021-1269) and monoclinic V_5S_8 (lattice parameters $a = 11.36$ Å, $b = 6.65$ Å and $c = 11.30$ Å, space group $F2/m$, JCPDS card no. 01-081-1596). Subsequent TEM analysis also revealed that the as-grown bulk product was a mixture of VS_2 and V_5S_8 (Fig. S1 of ESI). However, after low-temperature vacuum annealing treatment, while the peaks related to V-excess V-S compounds were suppressed, the XRD patterns of trigonal VS_2 were enhanced, attributed to facile desulfurization at low temperature.[44] Specifically, the predominant peaks reflected the property of layered materials with van der Waals (vdW) gaps along the c-axis. The estimated thickness of monolayer VS_2 was 5.72 Å, calculated by the (001) peak position from XRD data, in good agreement with the JCPDS card reference.

Fig. 1c shows the Raman spectrum of the annealing-treated VS_2 crystal, which has peaks in the range of 100 to 500 cm^{-1}. The three observed Raman peaks are quite similar to those of a previous report,[46] where the A_1 out-of-plane vibration mode at ~330 cm^{-1}, the E_2 in-plane vibration mode at ~260 cm^{-1}, and two-phonon signals in the range of 150-200 cm^{-1} were assigned. To accurately define the chemical composition of the as-grown bulk VS_2, XPS characterization was performed. Fig. 1d reveals that the chemical compositions obtained from the XPS measurements of VS_2 bulk crystals were composed of only the chemical states, V^{4+} 2p and S^{2-} 2p. The V:S atomic ratio derived from the XPS result was calculated to be 1:1.98.

A small bump in the V spectrum may be attributed to the lower possibility of partially intercalated V atoms.

Similar to conventional mechanical exfoliations, thin flakes of VS_2 were obtained from the bulk crystal by blue tape. After repeated peeling to form appropriate thin crystals of VS_2, we selected one of them, and the thickness was measured by AFM, as shown in Fig. 2a. The selected VS_2 flakes showed uniform and smooth surfaces in the AFM topography. The thickness of the VS_2 flakes was measured to be ~ 4 nm, indicating 7 layers of VS_2. While most TMDCs can be exfoliated mechanically to allow very thin flakes, some layered materials do not peel off easily. The calculated exfoliation energy, the difference in energy per atom between the monolayer and bulk, can be a rough guide (200 meV/atom, for example) to identify the feasibility of exfoliation.[47] The exfoliation energy of VS_2 is somewhat higher than graphene and other chalcogen 2D materials, hindering the preparation of large and regularly shaped flakes. To identify the crystal structure and elemental composition, TEM measurements were performed, as shown in Fig. 2b. Though irregular shape (low resolution TEM image, left of Fig. 2b), atomic ratio between V and S, clear lattice fringe, and fast Fourier transform from HR-TEM confirm the single crystalline nature of VS_2 with a stoichiometric composition (see Table S1 in ESI). The lattice spacings of 0.20 Å and 0.16 Å match the (102) and (110) planes of trigonal VS_2, respectively.

Fig. 2c illustrates the ball and stick model of the top and side views of the symmetric trigonal 1T-phase VS_2. Figs. 2d and e show representative HAADF-STEM images of the top surface and cross-section of 1T-VS_2, respectively. The top surface of 1T-VS_2 clearly exhibited a perfect honeycomb lattice without visible defects, indicating excellent single crystallinity. The exact position of both V and S can be identified as the intensity in the HAADF image being proportional to the atomic number due to the scattered electron beams from the specimen's

atoms.[48] The yellow dashed line in Fig. 2d is along the (110) plane, and the corresponding intensity profile is shown in the inset. The calculated in-plane lattice constant a = 3.25 Å (5.63/√3) is in agreement with a previous report.[38] As shown in Fig. 2e, the out-of-plane lattice constant c and vdW gap size were estimated to be 5.85±0.15 and 2.78±0.07 Å, respectively. Note that the zone axis of the STEM images deviated from the a-axis to acquire clear HAADF images.

Since in-depth structural analysis of perfect stoichiometric VS_2, especially simultaneous studies of CDW state, is rare, investigating the charge-distributed structure is worthy of academic research. To explore the structural and electronic properties, we studied the high-quality VS_2 single crystal using STM. Fig. 3a shows the STM topographic image of the as-cleaved VS_2 crystal, where ordered structures were observed. Fig. 3b exhibits the enlarged STM image of the VS_2 terrace marked as a red dashed box in Figure 3a, measured at a sample bias voltage (V_{bias}) of -50 mV. To understand the CDW orders in VS_2, we performed the fast Fourier transformation (FFT) of the STM image. In addition to the lattice peaks ($\mathbf{q}_{Bragg}$), two distinct charge modulation vectors denoted by $\mathbf{q}_1$ and $\mathbf{q}_2$ were observed in Fig. 3c, where green, yellow, and magenta circles indicate $\mathbf{q}_1$, $\mathbf{q}_2$, and the Bragg vector ($\mathbf{q}_{Bragg}$), respectively. The charge ordering patterns were predominantly regular, with minor local deviations mainly due to the surface defects.

We will now discuss the CDW vectors in detail. As seen in the left panel of Fig. 4a, $\mathbf{q}_1$ is positioned at the 0.67 $\overline{\Gamma K}$ position in the first Brillouin zone (FBZ), which is consistent with the CDW vector $\mathbf{q}$ = (0.22, 0.22, 0) reported in a previous TEM study of Li deintercalated bulk VS_2.[34] To understand the origin of the CDW peak of $\mathbf{q}_1$, we checked whether a nesting condition could be satisfied on the Fermi surface. Fig. 4b shows the Fermi surface of our VS_2 crystals measured by ARPES. The orange line indicates the magnitude of $\mathbf{q}_1$. From the scale,

it is evident that $\mathbf{q}_1$ cannot be matched to any nesting vectors on the Fermi surface. The newly emerged CDW vector $\mathbf{q}_2$, on the other hand, is located at 0.50 $\overline{\Gamma M}$, which corresponds to $\mathbf{q}$ = (0.25, 0, 0) or equivalently $\mathbf{q}$ = (0, 0.25, 0) in the reciprocal lattice coordinate in the right panel of Fig. 4a. The CDW vector $\mathbf{q}_2$ also cannot be matched to the nesting vectors aligned along $\overline{\Gamma M}$ in Fig. 4b.

DFT calculations of the phonon dispersions for the bulk 1T-VS_2 crystal confirm the structural instabilities and the corresponding softened phonon modes along the respective directions in momentum space. Fig. 4c displays the calculated phonon spectra weighted by a 9×9×1 supercell of VS_2. A previous study on the VS_2 monolayer reported the instability of acoustic phonon dispersion at $\mathbf{q}$ = 2/3 $\overline{\Gamma K}$ and 1/2 $\overline{\Gamma M}$ wavevectors, which correspond to transverse- and longitudinal-acoustic branches, respectively.[49] We constructed a 9×9×1 supercell for the small $\mathbf{q}$ shift in different directions. The displaced atoms in the supercell structure exhibit structural instability in phonon dispersion, which corresponds to the CDW state. Moreover, the CDW vectors $\mathbf{q}$s observed at 0.67 $\overline{\Gamma K}$ and 0.50 $\overline{\Gamma M}$ in bulk VS_2 are similar to those of previous research from the density functional perturbation theory (DFPT) method. Phonon softening modes with imaginary frequencies at $\mathbf{q}$s were clearly exhibited, indicating phonon instabilities in momentum space. The dominant instabilities are located at approximately $\mathbf{q}_1$ = 0.62 $\overline{\Gamma K}$ and 0.48 $\overline{\Gamma M}$, qualitatively consistent with the experimentally observed $\sqrt{6} \times \sqrt{6}$R30° and 4×4 CDW orders, respectively. According to our first-principles calculations, very large vibrational amplitudes of the V atoms can lead to the instability of the phonon mode. The displacements of the V atoms are more significant than those of S atoms for the modulated structure with an imaginary frequency when compared to the VS_2 structure in equilibrium. For further view, the electronic band structures of the bulk 1T-VS_2 obtained by

ARPES and DFT calculations were described at electronic supplementary information (Fig. S2).

The unconventional nature of the CDW vectors ($\mathbf{q}_1$ and $\mathbf{q}_2$) can be supported by the STM images measured at opposite bias polarities. When a conventional Peierls-like distortion induces a CDW phase, the energy band splits in a bonding-antibonding fashion with a CDW gap opening, resulting in the inverted contrast of STM images due to the flipped bias polarity around the CDW gap.[50-52] Fig. 5a shows the STM image measured at V_{bias} = 50 mV. Compared with that of the STM image measured at V_{bias} = -50 mV, the image contrast remains the same regardless of the bias polarity, supporting that the bonding-antibonding band splitting does not cause the CDW gap opening. Other STM topographic and FFT images with various biases are shown in Fig. S3 (ESI). As shown in Fig. 5b, we determined that the CDW gap (Δ) of our VS_2 crystal is $2\Delta \approx 130$ meV at 15 K. In a very recent result on the local STS spectra of monolayer VS_2, the CDW gap was fully open in the unoccupied states at 7 K and then exhibited flat conductance at higher temperatures, associated with strong electron-electron correlations caused by large lattice distortions.[49] In our bulk VS_2 case, however, a "V"-shaped gap with a finite value, namely, a soft CDW gap, implies a partially gapped Fermi surface.[11]

A CDW instability can be established by effective phonon softening that induces Kohn anomalies at the CDW vector $\mathbf{q}$; $\omega_{ren}^2 = \omega_q^2 - \frac{2g^2\omega_q}{\hbar}|\chi(q)|$, where ω_{ren} is the renormalized phonon frequency, ω_q is the phonon frequency, g is the electron-phonon coupling constant, $\hbar$ is the Planck constant and $\chi(q)$ is the electron-hole polarizability.[53] Given that the nesting condition is missing in VS_2, $\chi(q)$ should be small. Therefore, the CDW instability condition ($\omega_{ren}^2 = 0$) can only be satisfied by strong electron-phonon coupling. In this case, the the Bardeen–Cooper–Schrieffer (BCS) theory can support the thermodynamic phase transition of the CDW. By the mean-field approximation of 1D electron-phonon Hamiltonian, the relation

between the CDW gap and transition temperature (T_{CDW}) is given by $\Delta = 1.76\ k_B T_{CDW}$, where k_B is the Boltzmann constant.[54] The estimated T_{CDW} according to BCS theory is approximately 460 K. However, Fig. 5b shows that Δ is already closed at 300 K, implying that the electron-phonon coupling in VS_2 is larger than the BCS assumption.

Conclusion

In summary, we demonstrated a facile approach for fabricating high-quality single crystalline 1T-VS_2 bulk crystals and their multiple CDW states. Spectroscopic and microscopic evidence confirmed that the metastable phase comprising VS_2 and V_5S_8 turns into a perfect stoichiometric VS_2 due to desulfurization via vacuum annealing at low temperature. In these VS_2 single crystals, multiple charge modulation vectors, including a Bragg vector, were observed with $\sqrt{6} \times \sqrt{6}$R30° and 4×4 CDW orders at 0.67 $\overline{\Gamma K}$ and 0.50 $\overline{\Gamma M}$, respectively. These CDW states were characterized by not only the absence of nesting vectors on the Fermi surface but also a lack of contrast inversion in regard to bias polarity. The DFT calculations adopted with the supercell of VS_2 showed the imaginary frequency in phonon softening modes, implying phonon instability in a momentum space. The fabrication strategy and the atomic fine structure of the VS_2 bulk crystals may shed significant light on the exotic CDW system in V-based layered materials.

Experimental section

Fabrication of single crystalline VS_2

V (99.5% pure) and S powder (99.999% pure) were used as sources in a stoichiometric amount of 2:1 wt%. VCl_3 powder (99% pure) as a transporting agent (concentration of 1.5 mg/cm^3)

was used to provide sufficient vapor pressure. The mixture of sources and transporting agent was placed in a sealed quartz ampule under high vacuum, located at the center between two independent heating zones of a furnace as shown in Fig. 1a. Two heating zones for the forward reaction (T_1) and crystallization reaction (T_2) were heated slowly in five steps to approach their maximum temperatures, 920 °C and 850 °C, respectively. After 72 hours at the maximum temperatures, the system was cooled naturally, and shiny silver crystals were collected. Low-temperature annealing treatment was performed in a high-vacuum chamber system. The temperature was ramped up to 180 °C in 5 min and maintained under ~10^{-6} Torr. After 1 hour, the furnace was cooled to room temperature naturally under the same working pressure.

Characterization of VS_2

The VS_2 bulk crystals were characterized by using X-ray photoelectron spectroscopy (XPS), X-ray diffraction (XRD), Raman spectroscopy, high-resolution tunneling electron microscopy (HR-TEM) and high-angle annular dark-field scanning transmission electron microscopy (HAADF-STEM) combined with energy-dispersive X-ray spectroscopy (EDS). Cross-sectional high-angle annular dark-field (HAADF) STEM images were obtained after cutting the crystal by using a focus ion beam (FIB). Mechanical exfoliation was performed by peeling off as-grown crystals by using a simple blue-tape method. Exfoliated crystals were transferred onto fresh Si/SiO_2 substrates, and atomic force microscopy (AFM) was performed on the exfoliated crystals to measure the thickness.

STM measurements

STM measurements were performed using a cryogen-free low temperature STM (PanScan Freedom, RHK Techonolgy) with a base temperature of 15 K. The VS_2 crystal was glued to the sample holder and cleaved at room temperature in an ultrahigh vacuum (UHV) chamber. The cleaved sample was immediately inserted into the STM head at 15 K or 300 K. In the

scanning tunneling spectroscopy (STS) measurements, we used a standard lock-in technique with a modulation frequency of f = 342 Hz and modulation amplitude of V_{mod} = 5 mV.

ARPES measurements

Angle-resolved photoemission spectroscopy (ARPES) measurements were performed in a micro-ARPES end-station (base pressure of ~3×10^{-11} Torr) at the MAESTRO facility at beamline 7.0.2 at the Advanced Light Source, Lawrence Berkeley National Laboratory. The ARPES system was equipped with a Scienta R4000 electron analyzer. The lateral size of the synchrotron beam was estimated to be between 30 and 50 μm. VS_2 single crystals were cleaved in situ at 20 K to obtain clean surfaces and kept below 20 K during the ARPES measurements. The total energy and angular resolution of our experiments were better than 20 meV and 0.1° for the photon energy of 106 eV to 156 eV, respectively.

DFT calculations

To investigate the electronic properties of the VS_2 bulk structure, we used the Vienna *ab initio* simulation package (VASP) based on density functional theory (DFT).[55,56] A plane-wave basis set was adopted to expand the electronic wavefunctions. The interactions between the electrons and ions were described using the projector-augmented-wave (PAW) method.[57,58] The exchange-correlation energy was modeled using the Perdew-Burke-Ernzerhof (PBE) type generalized gradient approximation (GGA) function.[59] The kinetic energy cutoff was 650 eV, and a Γ-centered 18×18×18 *k*-point grid was used for the electronic structure calculations. The convergence tolerance of energy was 10^{-6} eV. Grimme's DFT-D3 method was used for van der Waals correction.[60] We used the Phonopy package for the phonon calculation and performed it by the finite displacement method.[61] We constructed a 9×9×1 supercell for the phonon

calculation. The kinetic energy cutoff was the same as the unit-cell calculation, whereas a Γ-centered 1×1×12 *k*-point grid was used for the 9×9×1 supercell.

Supplementary Information

Electronic supplementary information (ESI) available. HRTEM analysis of as-grown bulk product before vacuum annealing treatment, and STM topographic images and their FFT with various bias voltages. See DOI: https://doi.org/10.1039/.

Author Contributions

J.S. and S.L. planned and supervised the project. S.L. and S.H.C. fabricated and characterized VS_2 bulk crystals. S.H.L. conducted STM measurements with assistance of J.S. Y.C.P. and M.J. performed TEM measurements. J.C. and G.K. carried out DFT calculations. H.J.K., B.K.C., I.H.L. Y.J.C. performed ARPES measurements. S.H.L., J.C., G.K., J.S., and S.L. cowrote the manuscript. All authors have given approval to the final version of the manuscript and commented on the manuscript.

Conflicts of Interest

The authors declare no conflict of interest.

Acknowledgements

This work was supported by the National Research Foundation (NRF) grants (NRF-2020R1A2C200373211, 2021R1A6A3A14040322, 2021R1F1A1050726), the Basic Science Research Program's financial support (NRF-2020R1A6A1A03043435), and the CoE program (19-CoE-NT-01, 20-CoE-NT-02) at DGIST funded by the Korean government. I.H.L. was supported by the KIST Institutional Program and National Research Council of Science and Technology (CAP-16-01-KIST) and MOLIT as [Innovative Talent Education Program for Smart City]. The Advanced Light Source is supported by the Director, Office of Science, Office of Basic Energy Sciences, of the U.S. Department of Energy under contract no. DE-AC02-05CH11231.

REFERENCES

1. M. Chhowalla, D. Jena and H. Zhang, Two-dimensional semiconductors for transistors, *Nat. Rev. Mater.*, 2016, **1**, 16052.

2. A. J. Mannix, B. Kiraly, M. C. Hersam and N. P Guisinger, Synthesis and chemistry of elemental 2D materials, *Nat. Rev. Chem.*, 2017, **1**, 0014.

3. S. Manzeli, D. Ovchinnikov, D. Pasquier, O. V. Yazyev and A. Kis, 2D transition metal dichalcogenides, *Nat. Rev. Mater.*, 2017, **2**, 17033.

4. W. Choi, N. Choudhary, G. H. Han, J. Park, D. Akinwande and Y. H. Lee, Recent development of two-dimensional transition metal dichalcogenides and their applications, *Mater. Today*, 2017, *20*, 116-130.

5. M. M. Ugeda, A. J. Bradley, Y. Zhang, S. Onishi, Y. Chen, W. Ruan, C. Ojeda-Aristizabal, H. Ryu, M. T. Edmonds, H.-Z. Tsai, A. Riss, S.-K. Mo, D. Lee, A. Zettl, Z. Hussain and

Z.-X. Shen, Crommie, M. F. Characterization of collective ground states in single-layer $NbSe_2$, *Nat. Phys.*, 2016, **12**, 92-97.

6. D. A. Rhodes, A. Jindal, N. F. Q. Yuan, Y. Jung, A. Antony, H. Wang, B. Kim, Y. Chiu, T. Taniguchi, K. Watanabe, K. Barmak, L. Balicas, C. R. Dean, X. Qian, L. Fu, A. N. Pasupathy and J. Hone, Enhanced superconductivity, in monolayer T_d-$MoTe_2$, *Nano Lett.*, 2021, **21**, 2505-2511.

7. H. Dai, H. Cheng, M. Cai, Q. Hao, Y. Xing, H. Chen, X. Chen, X. Wang and J.-B. Han, Enhancement of the coercive field and exchange bias effect in $Fe_3GeTe_2/MnPX_3$ (X = S and Se) van der Waals heterostructures, *ACS Appl. Mater. Interfaces*, 2021, **13**, 24314-24320.

8. N. H. Lam, P. L. Nguyen, B. K. Choi, T. T. Ly, D. Duvjir, T. G. Rhee, Y. J. Jo, T. H. Kim, C. Jozwiak, A. Bostwick, E. Rotenberg, Y. Hwang, Y. J. Chang, J. Lee and J. Kim, Controlling spin-orbit coupling to tailor type-II Dirac bands, *ACS Nano*, 2022, **16**, 11227-11233.

9. Z. Guguchia, A. Kerelsky, D. Edelberg, S. Banerjee, F. von Rohr, D. Scullion, M. Augustin, M. Scully, D. A. Rhodes, Z. Shermadini, H. Luetkens, A. Shengelaya, C. Baines, E. Morenzoni, A. Amato, J. C. Hone, R. Khasanov, S. J. L. Billinge, E. Santos, A. N. Pasupathy and Y. J. Uemura, Magnetism in semiconducting molybdenum dichalcogenides, *Sci. Adv.*, 2018, **4**, eaat3672.

10. W. Fu, J. Qiao, X. Zhao, Y. Chen, D. Fu, W. Yu, K. Leng, P. Song, Z. Chen, T. Yu, S. J. Pennycook, S. Y. Quek and K. P. Loh, Room temperature commensurate charge density wave on epitaxially grown bilayer 2*H*-tantalum sulfide on hexagonal boron nitride, *ACS Nano*, 2020, **14**, 3917-3926.

11. D. Zhang, J. Ha, H. Baek, Y.-H. Chan, F. D. Natterer, A. F. Myers, J. D. Schumacher, W. G. Cullen, A. V. Davydov, Y. Kuk, M. Y. Chou, N. B. Zhitenev and J. A. Stroscio, Strain engineering a $4a\times\sqrt{3}a$ charge-density-wave phase in transition-metal dichalcogenide 1*T*-VSe_2, *Phys. Rev. Mater.*, 2017, **1**, 024005.

12. M. Liu, C. Wu, Z. Liu, Z. Wang, D.-X. Yao and D. Zhong, Multimorphism and gap opening of charge-density-wave phases in monolayer VTe_2, *Nano Res.*, 2020, **13**, 1733-1738.

13. S. V. Borisenko, A. A. Kordyuk, V. B. Zabolotnyy, D. S. Inosov, D. Evtushinsky, B. Büchner, A. N. Yaresko, A. Varykhalov, R. Follath, W. Eberhardt, L. Patthey and H. Berger, Two energy gaps and Fermi-surface "Arcs" in $NbSe_2$, *Phys. Rev. Lett.*, 2009, **102**, 166402.

14. K. Sugawara, Y. Nakata, K. Fujii, K. Nakayama, S. Souma, T. Takahashi and T. Sato, Monolayer VTe_2: Incommensurate Fermi surface nesting and suppression of charge density waves, *Phys. Rev. B*, 2019, **99**, 241404.

15. A. Soumyanarayanan, M. M. Yee, Y. He, J. van Wezel, D. J. Rahn, K. Rossnagel, E. W. Hudson, M. R. Norman and J. E, Hoffman, Quantum phases transition from triangular to stripe charge order in $NbSe_2$, *Proc. Natl. Acad. Sci.*, 2013, **110**, 1623-1627.

16. C. Lian, S.-J. Zhang, S.-Q. Hu, M.-X. Guan and S. Meng, Ultrafast charge ordering by self-amplified exciton-phonon dynamics in $TiSe_2$, *Nat. Commun.*, 2020, **11**, 43.

17. Y. Umemoto, K. Sugawara, Y. Nakata, T. Takahashi and T. Sato, Pseudogap, Fermi arc, and Peierls-insulating phase induced by 3D-2D crossover in monolayer VSe_2, *Nano Res.*, 2019, **12**, 165-169.

18. G. Duvjir, B. K. Choi, I. Jang, S. Ulstrup, S. Kang, T. T. Ly, S. Kim, Y. H. Choi, C. Jozwiak, A. Bostwick, E. Rotenberg, J.-G. Park, R. Sankar, K.-S. Kim, J. Kim and Y. J. Chang,

Emergence of a metal-insulator transition and high-temperature charge-density waves in VSe_2 at the monolayer limit, *Nano Lett.*, 2018, **18**, 5432-5438.

19. H. Luo, W. Xie, J. Tao, H. Inoue, A. Gyenis, J. W. Krizan, A. Yazdani, Y. Zhu and R. J. Cava, Polytypism, polymorphism, and superconductivity in $TaSe_{2-x}Te_x$, *Proc. Natl. Acad. Sci.*, 2015, **112** 1174-1180.

20. P. He, M. Yan, G. Zhang, R. Sun, L. Chen, Q. An and L. Mai, Layered VS_2 nanosheet-based aqueous Zn ion battery cathode, *Adv. Energy Mater.*, 2017, **7**, 1601920.

21. W. Zhao, B. Dong, Z. Guo, G. Su, R. Gao, W. Wang and L. Cao, Colloidal synthesis of VSe_2 single-layer nanosheets as novel electrocatalysts for the hydrogen evolution reaction, *Chem. Commun.*, 2016, **52**, 9228-9231.

22. Y. Wang, Z. Sofer, J. Luxa and M. Pumera, Lithium exfoliated vanadium dichalcogenides (VS_2, VSe_2, VTe_2) exhibit dramatically different properties from their bulk counterparts, *Adv. Mater. Interfaces*, 2016, **3**, 1600433.

23. M. Bonilla, S. Kolekar, Y. Ma, H. C. Diaz, V. Kalappattil, R. Das, T. Effers, H. R. Gurierrez, M.-H. Phan and M. Batzill, Strong room-temperature ferromagnetism in VSe_2 monolayers on van der Waals substrates, *Nat. Nanotechnol.*, 2018, **13**, 289-293.

24. N. Mitsuishi, Y. Sugita, M. S. Bahramy, M. Kamitani, T. Sonobe, M. Sakano, T. Shimojima, H. Takahashi, H. Sakai, K. Horiba, H. Kumigashira, K. Taguchi, K. Miyamoto, T. Okuda, S. Ishiwata, Y. Motome and K. Ishizaka, Switching of band inversion and topological surface states by charge density wave, *Nat. Commun.*, 2020, **11**, 2466.

25. H. J. Kim, B. K. Choi, I. H. Lee, M. J. Kim, S.-H. Chun, C. Jozwiak, A. Bostwick, E. Rotenberg and Y. J. Chang, Electronic structure and charge-density wave transition in monolayer VS_2, *Cur. Appl. Phys.*, 2021, **30**, 8-13.

26. D. Won, D. H. Kiem, H. Cho, D. Kim, Y. Kim, M. Y. Jeong, C. Seo, J. Kim, J.-G. Park, M. J. Han, H. Yang and S. Cho, Polymorphic spin, charge, and lattice waves in vanadium ditelluride, *Adv. Mater.*, 2020, **32**, 1906578.

27. J. Diego, A. H. Said, S. K. Mahatha, R. Bianco, L. Monacelli, M. Calandra, F. Mauri, K. Rossnagel, I. Errea and S. Blanco-Canosa, Van der Waals driven anharmonic melting of the 3D charge density wave in VSe_2, *Nat. Commun.*, 2021, **12**, 598.

28. K. Tsutsumi, X-ray-diffraction study of the periodic lattice distortion associated with a charge-density wave in 1*T*-VSe_2, *Phys. Rev. B*, 1982, **26**, 5756-5759.

29. K. Terashima, T. Sato, H. Komatsu and T. Takahashi, Charge-density wave transition of 1*T*-VSe_2 studied by angle-resolved photoemission spectroscopy, *Phys. Rev. B*, 2003, **68**, 155108.

30. V. N. Strocov, M. Shi, M. Kobayashi, C. Monney, X. Wang, J. Krempasky, T. Schmitt, L. Patthey, H. Berger and P. Blaha, Three-dimensional electron realm in VSe_2 by soft-X ray photoelectron spectroscopy: Origin of charge-density waves, *Phys. Rev. Lett.*, 2012, **109**, 086401.

31. Y. Wang, J. Ren, J. Li, Y. Wang, H. Peng, P. Yu, W. Duan and S. Zhou, Evidence of charge density wave with anisotropic gap in a monolayer VTe_2 film, *Phys. Rev. B*, 2019, **100**, 241404(R).

32. T. Ohtani, K. Hayashi, M. Nakahira and H. Nozaki, Phase transition in $V_{1+x}Te_2$ ($0.04 \leq x \leq 0.11$), *Solid State Coomun.*, 1981, **40**, 629-631.

33. C. J. Sayers, L. S. Farrar, S. J. Bending, M. Cattelan, A. J. H. Jones, N. A. Fox, G. Kociok-Köhn, K. Koshmak, J. Laverock, L. Pasquali and E. Da Como, Correlation between crystal purity and the charge density wave in 1*T*-VSe_2, *Phys. Rev. Mater.*, 2020, **2**, 025002.

34. M. Mulazzi, A. Chainani, N. Katayama, R. Educhi, M. Matsunami, H. Ohashi, Y. Senba, M. Nohara, M. Uchida, H. Takagi and S. Shin, Absence of nesting in the charge-density-wave system 1*T*-VS_2 as seen by photoelectron spectroscopy, *Phys. Rev. B*, 2010, **82**, 075130.

35. A. Gauzzi, A, Sellam, G. Rousse, Y. Klein, D. Taverna, P. Giura, M. Calandra, G. Loupias, F. Gozzo, E. Gilioli, F. Bolzoni, G. Allodi, R. De Renzi, G. L. Calestani and P. Roy, Possible phase separation and weak localization in the absence of a charge-density wave in single-phase 1*T*-VS_2, *Phys. Rev. B*, 2014, **89**, 235125.

36. W. Bensch and J. Koy, The single crystal structure of V_5S_8 determined at two different temperatures: anisotropic changes of the metal atom network, *Inorg. Chim. Acta*, 1993, **206**, 221-223.

37. H. Moutaabbid, Y. L. Godec, D. Taverna, B. Baptiste, Y. Klein, G. Loupias, and A. Gauzzi, High-pressure control of vanadium self-intercalation and enhanced metallic properties in 1*T*-$V_{1+x}S_2$ single crystals, *Inorg. Chem.*, 2016, **55**, 6481-6486.

38. Q. Ji, C. Li, J. Wang, J. Niu, Y. Gong, Z. Zhang, Q. Fang, Y. Zhang, J. Shi, L. Liao, X. Wu, L. Gu, Z. Liu and Y. Zhang, Metallic vanadium disulfide nanosheets as a platform material for multifunctional electrode applications, *Nano Lett.*, 2017, **17**, 4908-4916.

39. Y. Guo, H. Deng, X. Sun, X. Li, J. Zhao, J. Wu, W. Chu, S. Zhang, H. Pan, X. Zheng, X. Wu, C. Jin, C. Wu and Y. Xie, Modulation of metal and insulator states in 2D ferromagnetic VS_2 by van der Waals interaction engineering, *Adv. Meter.*, 2017, **29**, 1700715.

40. X. Sun, T. Yao, Z. Hu, Y. Guo, Q. Liu, S. Wei and C. Wu, *In situ* unravelling structural modulation across the charge-density-wave transition in vanadium disulfide, *Phys. Chem. Chem. Phys.*, 2015, **17**, 13333-13339.

41. H. Xu, M.-C. Hsu, H.-R. Fuh, J. Feng, X. Han, Y. Zhao, D. Zhang, X. Wang, F. Liu, H. Liu, J. Cho, M. Choi, B. S. Chun, C. Ó. Coileáin, Z. Wang, M. B. A. Jalil, H.-C. Wu and C.-R. Chang, Threshold magnetoresistance in anisotropic magnetic 2D transition metal dichalcogenides, *J. Mater. Chem. C*, 2018, **6**, 3058-3064.

42. M. Hossain, J. Wu, W. Wen, H. Liu, X. Wang and L. Xie, Chemical vapor deposition of 2D vanadium disulfide and diselenide and Raman characterization of the phase transitions, *Adv. Mater. Interfaces*, 2018, **5**, 1800528.

43. P. Raybaud, J. Hafner, G. Kresse and H. Toulhoat, H. *Ab initio* density functional studies of transition-metal sulphides: II. Electronic structure, *J. Phys.: Condens. Matter*, 1997, **9**, 11107.

44. D. W. Murphy, C. Cros, F. J. Di Salvo and J. V. Waszczak, Preparation and properties of LixVS2 (0≤x≤1), *Inorg. Chem.*, 1977, **16**, 3027-3031.

45. M. Yokoyama, M. Yoshimura, M. Wakihara, S. Somiya and M. Yaniguchi, Synthesis of vanadium sulfides under high pressure, *J. Solid State Chem.*, 1985, **60**, 182-187.

46. J. Yuan, J. Wu, W. J. Hardy, P. Loya, M. Lou, Y. Yang, S. Najmaei, M. Jiang, F. Qin, K. Keyshar, H. Ji, W. Gao, J. Bao, J. Kono, D. Natelson, P. M. Ajayan and J. Lou, J. Facile synthesis of single crystal vanadium disulfide nanosheets by chemical vapor deposition for efficient hydrogen evolution reaction, *Adv. Mater.*, 2015, **27**, 5605-5609.

47. K. Choudhary, I. Kalish, R. Beams and F. Tavazza, High-throughput identification and characterization of two-dimensional materials using density functional theory, *Sci. Rep.*, 2017, **7**, 5179.

48. S. Lee, J. In, S. Kim, Y. C. Park, H. Kim, H. Yoon, J. Kim, S. Lee, B. Kim, B. Atomistrically observing real-space structure of composition modulated

$(Nb_{0.94}V_{0.06})_{10}(Si_xGe_{1-x})_7$ nanowires with ultralow resistivity, *J. Mater. Chem. C*, 2013, **1**, 1674-1679.

49. C. van Efferren, J. Berges, J. Hall, E. van Loon, S. Kraus, A. Schobert, T. Wekking, F. Huttmann, E. Plaar, N. Rothenbach, K. Ollefs, L. M. Arruda, N. Brookes, G. Schönhoff, K. Kummer, H. Wende, T. Wehling and T. Michely, A full gap above the Fermi level: the charge density wave of monolayer VS_2, *Nat. Commun.*, 2021, **12**, 6837.

50. M. Spera, A. Scarfato, Á. Pásztor, E. Giannini, D. R. Bowler and Ch. Renner, Insight into the charge density wave gap from contrast inversion in topographic STM images, *Phys. Rev. Lett.*, 2020, **125**, 267603.

51. M.-Q. Ren, S. Han, J.-Q. Fan, L. Wang, P. Wang, W. Ren, K. Peng, S. Li, S.-Z. Wang, F.-W. Zheng, P. Zhang, F. Li, X. Ma, Q.-K. Xue and C.-L. Song, Semiconductor-metal phase transition and emergent charge density waves in 1T-ZrX_2 (X = Se, Te) at the two-dimensional limit, *Nano Lett.*, 2022, **22**, 476-484.

52. J. Dai, E. Calleja, J. Alldredge, X. Zhu, L. Li, W. Lu, Y. Sun, T. Wolf, H. Berger and K. McElroy, Microscopic evidence for strong periodic lattice distortion in two-dimensional charge-density systems, *Phys. Rev. B*, 2014, **89**, 165140.

53. J.-P. Pouget, The Peierls instability and charge density wave in one-dimensional electronic conductors, *C. R. Phys.*, 2016, **17**, 332-356.

54. G. Grüner, The dynamics of charge-density waves, *Rev. Mod. Phys.*, 1988, **60**, 1129-1181.

55. G. Kresse and J. Hafner, *Ab initio* molecular dynamics for liquid metals, *Phys. Rev. B*, 1993, **47**, 558.

56. G. Kresse and J. Furthmüller, Efficient iterative schemes for ab initio total-energy calculations using a plane-wave basis set, *Phys. Rev. B*, 1996, **54**, 11169.

57. G. Kresse and D. Joubert, From ultrasoft pseudopotentials to the projector augmented-wave method, *Phys. Rev. B*, 1999, **59**, 1758.

58. D. Hobbs, G. Kresse and J. Hafner, Fully unconstrained noncollinear magnetism within the projector augmented-wave method, *Phys. Rev. B*, 2000, **62**, 11556.

59. J. P. Perdew, K. Burke and M. Ernzerhof, Generalized gradient approximation made simple, *Phys. Rev. Lett.*, 1996, **77**, 3865.

60. S. Grimme, J. Antony, S. Ehrlich and H. Krieg, A consistent and accurate ab anitio parametrization of density functional dispersion correction (DFT-D) for the 94 elements H-Pu, *J. Chem. Phys.*, 2010, **132**, 154104.

61. A. Togo and I. Tanaka, First principles phonon calculations in materials science, *Scr. Mater.*, 2015, **108**, 1-5.

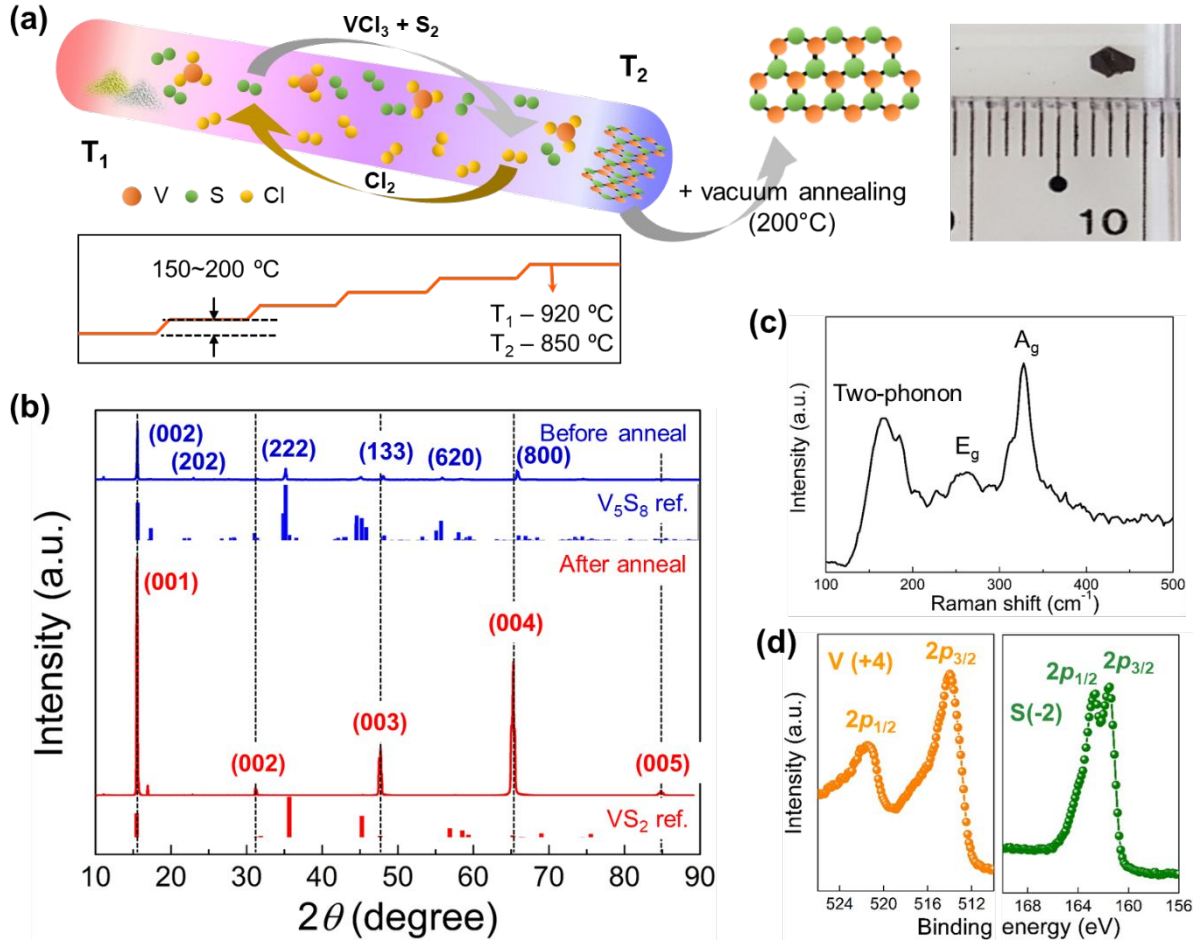

Fig. 1 (a) Schematic of VS_2 bulk crystal growth. Two heating zones (T_1 for sublimation temperature and T_2 for crystallization reaction temperature) were individually controlled in five steps. After the furnace was cooled naturally, corrected VS_2 bulk crystals were annealed at low temperature (200 °C) in a high-vacuum chamber. The right photograph indicates the final VS_2 bulk crystal. (b) XRD patterns of VS_2 bulk crystals before and after annealing treatment. While the peaks of VS_2 and V_5S_8 were observed before annealing, all the peaks after annealing were indexed to the trigonal 1T-VS_2 phase. The predominant peaks along the *c*-axis indicated the character of the van der Waals materials. (c) Raman spectra of 1T-VS_2 bulk crystals after annealing. (d) XPS spectra of V^{4+} and S^{2-} in 1T-VS_2 bulk crystals after annealing.

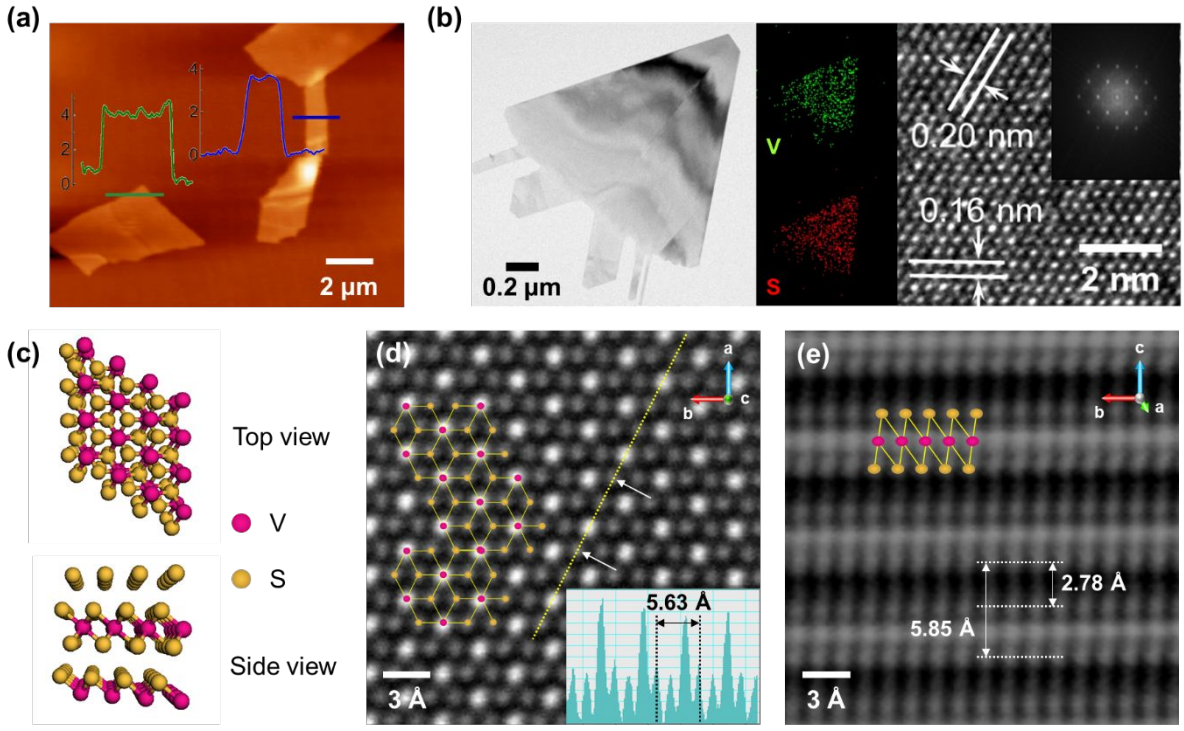

Fig. 2 (a) AFM topographic image of exfoliated 1T-VS_2 on a Si/SiO_2 substrate. The thickness profiles of the flakes are shown, corresponding to 7 layers of VS_2. (b) Low-magnification, enlarged high-resolution TEM images and corresponding EDS mapping of 1T-VS_2. The clear lattice fringes and the regular FFT configuration confirm the highly single crystalline nature. (c) Top and side views of the ball and stick model of the trigonal crystal structure of VS_2. (d, e) HAADF-STEM images of the top (d) and the cross-section of 1T-VS_2. Inset in (d) is the intensity profile along the yellow dashed line. The vdW gap between the VS_2 layers is clearly shown as ~5.85 Å.

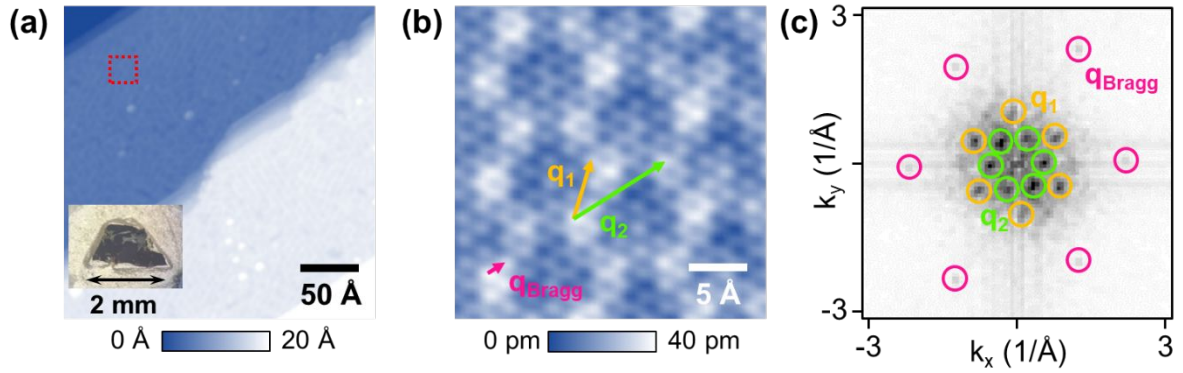

Fig. 3 (a) STM image of the cleaved VS_2 surface (V_b = -100 mV, I_t = -200 pA). The inset shows a photo of the cleaved VS_2 sample attached to the STM head. (b) Zoomed-in STM image highlighted by the red dashed rectangle in (a). $\mathbf{q}_{Bragg}$, $\mathbf{q}_1$, and $\mathbf{q}_2$ denote the basis vectors of the atomic lattice and two CDW lattices, respectively. A bias voltage of -50 mV was applied. (c) FFT of the topographic STM image in (b). The Bragg lattice peaks of 1T-VS_2 are marked by the outer six magenta circles. The inner six orange and green circles indicate the CDW peaks with $\sqrt{6} \times \sqrt{6}R30°$ and 4×4 order, respectively.

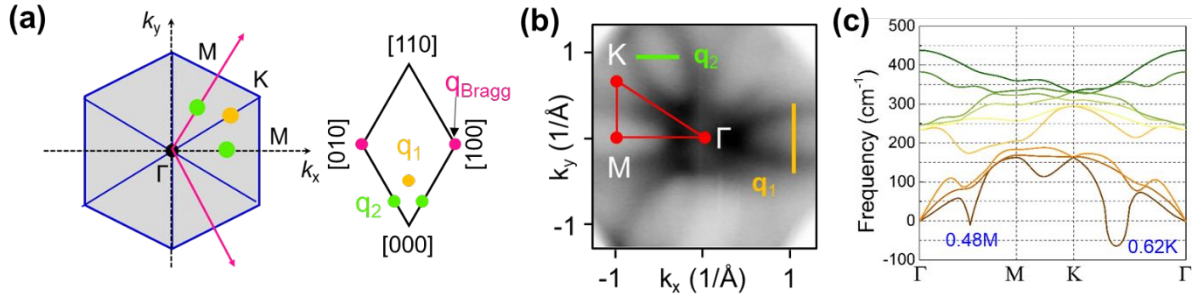

Fig. 4 (a) Schematic of the first hexagonal Brillouin zone (left) and the reciprocal unit cells (right). Orange and green colored circles indicate CDW vectors at the $\overline{\Gamma K}$ and $\overline{\Gamma M}$ planes, respectively. (b) Fermi surface map of the 1T-VS_2 bulk crystal obtained by ARPES at 15 K. Six cigar-shaped electron pockets centered at the M points are clearly shown on the K-Γ-M plane. (c) Phonon dispersion curve of the 9×9×1 supercell of 1T-VS_2. 0.62 $\overline{\Gamma K}$ and 0.48 $\overline{\Gamma M}$ represent the two prominent imaginary frequencies.

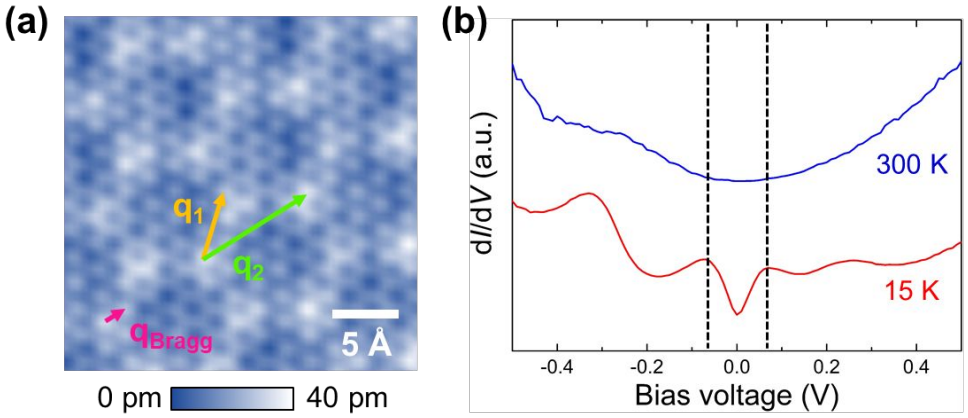

Fig. 5 (a) STM image of the same region in Figure 3(b) but with a bias voltage of 50 mV. (b) d*I*/d*V* spectra at 15 K and 300 K. The 2Δ CDW gap (~130 meV) is only observed at 15 K.